Finite element unit cell model based on ABAQUS for fiber reinforced composites

Tian Tang
Composites Manufacturing & Simulation Center, Purdue University
West Lafayette, IN 47906

1. Problem Statement

In this study, a finite element unit cell model was developed on the basis of ABAQUS to predict the effective thermo-mechanical properties of a fiber composite having three-phase interphase microstructure as shown in Fig. 1 in which the fiber is of circular and in a square array with a thin layer of interphase between the fiber and the matrix. The volume fractions of the fiber and interphase are 60% and 1%, respectively. The material properties of the constituents are presented in Table 1. Note that the fiber properties are orthotropic, despite the fact that all three Young's moduli and all three Poisson's ratios have been chosen to be the same. The materials of the matrix and interphase are isotropic. Finally, the local stresses within the unit cell were computed according to the prescribed macroscopic loadings. This report describes the detailed methodology used to obtain the effective properties and local fields using ABAQUS unit cell model.

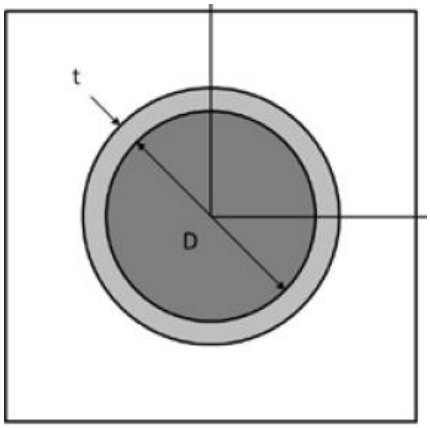

Fig. 1. Circular fiber and interphase between the fiber and the matrix.

2. Homogenization

The process of obtaining the effective properties of the composites is called homogenization. A variety of boundary and loading conditions and multiple run are required in order to obtain the full set effective properties and different local fields using ABAQUS finite element unit cell model.

Table 1. Material properties of constituents

Properties	Matrix	Fiber	Interphase
E (GPa)	350	450	5.0
υ	0.18	0.17	0.22
G (GPa)	148	171	2.0
α_{11} $(\frac{\mu}{^\circ C})$	64.8	-0.4	5.0
α_{22} $(\frac{\mu}{^\circ C})$	64.8	5.6	5.0
α_{33} $(\frac{\mu}{^\circ C})$	64.8	5.6	5.0

2.1 Periodic boundary conditions and effective properties

The composites can be idealized as assembly of many periodic unit cells to which the periodic boundary conditions are consequently applied, which means that the deformation mode in each unit cell are identical and there

is no gap or overlap between the adjacent unit cells. The periodic boundary conditions are represented as

$$u_i = \bar{\varepsilon}_{ij} x_j + v_i \tag{1}$$

where $\bar{\varepsilon}_{ij}$ is the average strain; v_i is the periodic part of the displacement components also called local fluctuation on the boundary surfaces. The displacements on a pair of opposite boundary surfaces are given by

$$u_i^{k+} = \bar{\varepsilon}_{ij} x_j^{k+} + v_i^{k+} \tag{2}$$

$$u_i^{k-} = \bar{\varepsilon}_{ij} x_j^{k-} + v_i^{k-} \tag{3}$$

where "$k+$" denotes along the positive x_j direction while "$k-$" means along the negative x_j direction. Since the periodic parts v_i^{k+} and v_i^{k-} are identical on the two opposite boundary surfaces of a periodic unit cell, the difference of Eq. (2) and (3) is obtained as

$$u_i^{k+} - u_i^{k-} = \bar{\varepsilon}_{ij}\left(x_j^{k+} - x_j^{k-}\right) = \bar{\varepsilon}_{ij} \Delta x_j \tag{4}$$

where Δx_j is actually the edge length of the unit cell.

Basically, ABAQUS unite cell modeling technique employs volume averaging process which means that the effective thermo-mechanical properties are linearly proportional to volume average stresses and strains of a unit cell and expressed as

$$\bar{\sigma}_{ij} = C^*_{ijkl} \bar{\varepsilon}_{kl} + C^*_{ijkl} \alpha^*_{ij} \theta \tag{5}$$

where C^*_{ijkl} is effective elastic stiffness; α^*_{ij} is the effective thermal expansion coefficient; θ is the temperature deviation; and the average stresses $\bar{\sigma}_{ij}$ and average strains $\bar{\varepsilon}_{kl}$ are defined as

$$\bar{\sigma}_{ij} = \frac{1}{\Omega} \int_{\Omega} \sigma_{ij} \, \mathrm{d}\Omega \tag{6}$$

$$\bar{\varepsilon}_{ij} = \frac{1}{\Omega} \int_{\Omega} \varepsilon_{ij} \, \mathrm{d}\Omega \tag{7}$$

with Ω being the volume of a periodic unit cell.

2.2 Finite element modeling

The periodic boundary conditions described in Eq. (4) are implemented into a python script. As shown in Fig. 2, the finite element unit cell model was meshed using 20 node brick element C3D20R. The fiber direction is along -1. Sweep mesh technique was used in order to obtain periodic mesh on opposite boundary surfaces, which means that the meshes on opposite boundary

surfaces are identical. The periodic boundary conditions described in Eq. (4) were applied to the unit cell by coupling opposite nodes on corresponding opposite boundary surfaces. In actual manipulation, three reference points are first created and their displacements are assigned as $\bar{\varepsilon}_{ij}\Delta x_j$. In the present study, the edge length of the unit cell along 1, 2, and 3 direction are respectively $\Delta x_1 = 0.1$ mm and $\Delta x_2 = \Delta x_3 = 1$ mm.

2.3 Numerical calculation of various effective thermo-mechanical properties

2.3.1 Calculation of E_{11}^*, υ_{12}^*, and υ_{13}^*

In the case of calculation of E_{11}, υ_{12}, and υ_{13}, the symmetric boundary conditions are imposed on 1-3, 2-3, and 1-2 planes, respectively, in order to eliminate rigid body rotation. The macroscopic strain $\bar{\varepsilon}_{11}$ along 1 direction was applied by prescribing the 1 direction displacement of the corresponding reference point. Since the 1 direction displacement of plane 2-3 is zero, the periodic boundary condition along -1 direction can be simplified as

$$u_1^{1+} = \bar{\varepsilon}_{11}\Delta x_1 \tag{8}$$

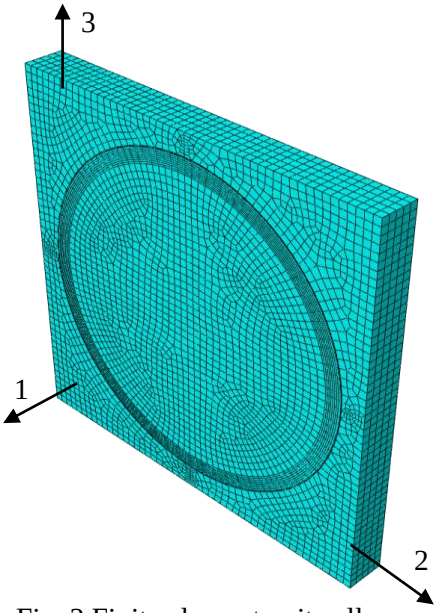

Fig. 2 Finite element unit cell model and coordinate system.

There are two ways to calculate the average stress $\bar{\sigma}_{11}$ generated by the imposed boundary and loading conditions. One way is to write a python script to obtain the stress and volume of each element and then the effective properties are equal to the summation of stress in each element divided by the total volume of the unit cell. Another simple but efficient way is to first obtain the summation of 1 component reaction force (RF_1) acting on the front boundary surface which is actual the 1 component of the reaction force of the corresponding reference point and can be obtained using the History Output as shown in Fig. 3. The average stress $\bar{\sigma}_{11}$ is equal to $\bar{\sigma}_{11} = {RF_1}/{A^{1+}}$ with A^{1+} being the area of the front boundary surface along 1 direction. The effective Young's modulus E_{11}^* is consequently computed as

$$E_{11}^* = \frac{\bar{\sigma}_{11}}{\bar{\varepsilon}_{11}} \tag{9}$$

For instance, the $\bar{\varepsilon}_{11}$ is 0.01 and $A^{1+} = 1\text{mm}^2$ in this study. The resultant RF_1 is 4.06557 N as shown in Fig. 3 such that $E_{11}^* = 406.557$ GPa.

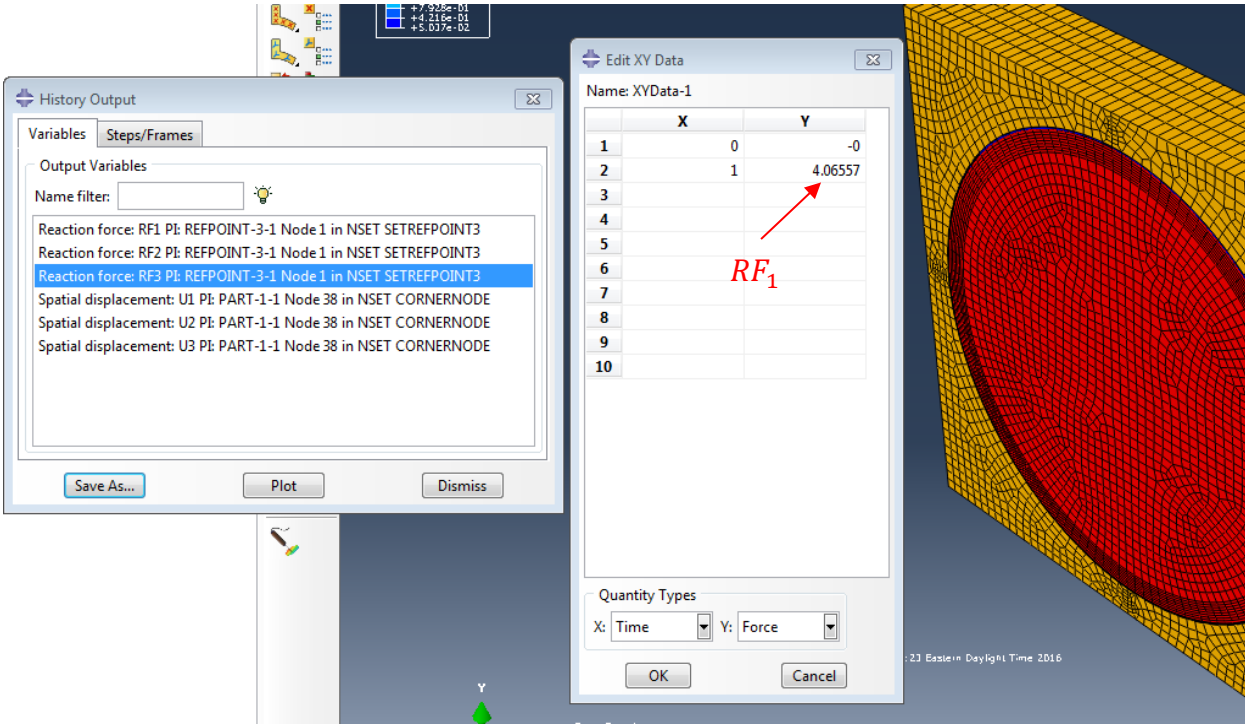

Fig. 3 The -1 component reaction force (RF_1) acting on the front boundary surface is actually the reaction force of the corresponding reference point.

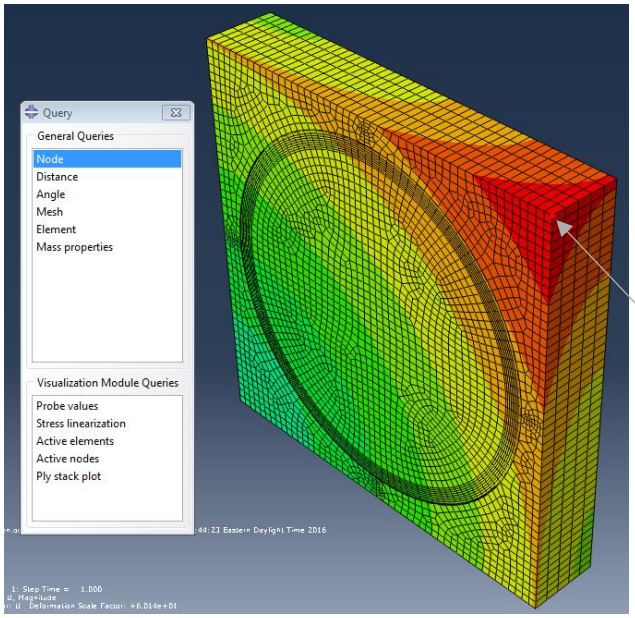

	u_3	u_2	u_1
Displacement (unscaled):	-1.74580e-003	-1.74580e-003	1.00000e-003

Fig. 4 Contour plot of displacement and the displacement of corner node.

The v_{12}^* and v_{13}^* are determined by tracking the displacement of corner node as shown in Fig. 4. In the present case, $v_{12}^* = -\frac{\bar{\varepsilon}_{22}}{\bar{\varepsilon}_{11}} = 0.17458$ and $v_{13}^* = v_{12}^*$.

2.3.2 Calculation of E_{22}^{*}, and υ_{23}^{*}

The symmetric boundary conditions are also needed to impose on 1-3, 2-3, and 1-2 planes, respectively, in order to eliminate rigid body rotation. The macroscopic strain $\bar{\varepsilon}_{22}$ along -2 direction was applied by assigning the -2 direction displacement of the corresponding reference point. Since the -2 direction displacement of plane 1-3 is zero, the periodic boundary condition along -1 direction can be simplified as

$$u_2^{2+} = \bar{\varepsilon}_{22}\Delta x_2 \tag{10}$$

The average stress $\bar{\sigma}_{22}$ is equal to $\bar{\sigma}_{22} = {RF_2}/{A^{2+}}$ with A^{2+} being the area of the right side boundary surface in 2 direction. The effective Young's modulus E_{22}^{*} is accordingly computed as

$$E_{22}^{*} = \frac{\bar{\sigma}_{22}}{\bar{\varepsilon}_{22}} \tag{11}$$

For instance, the $\bar{\varepsilon}_{22}$ is 0.01 and $A^{2+} = 0.1\text{mm}^2$ in this study. The resultant RF_2 is 0.27684 N as shown in Fig. 5 such that $E_{22}^{*} = 276.84$ GPa.

The υ_{23}^{*} is determined according to the displacements of corner node which are $u_2 = -0.00203529$ mm and $u_3 = 0.001$ mm such that the transverse Poisson's ratio is calculated as $\upsilon_{23}^{*} = -\frac{\bar{\varepsilon}_{33}}{\bar{\varepsilon}_{22}} = 0.203529$.

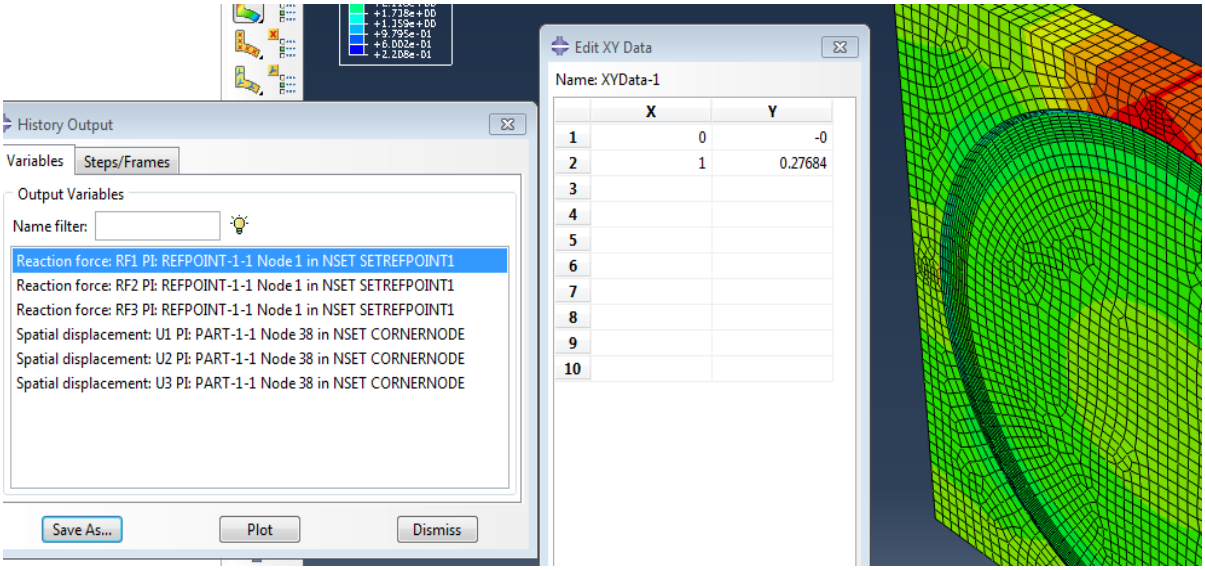

Fig. 5 The -2 component reaction force (RF_2) acting on the side boundary surface is actually the reaction force of the corresponding reference point.

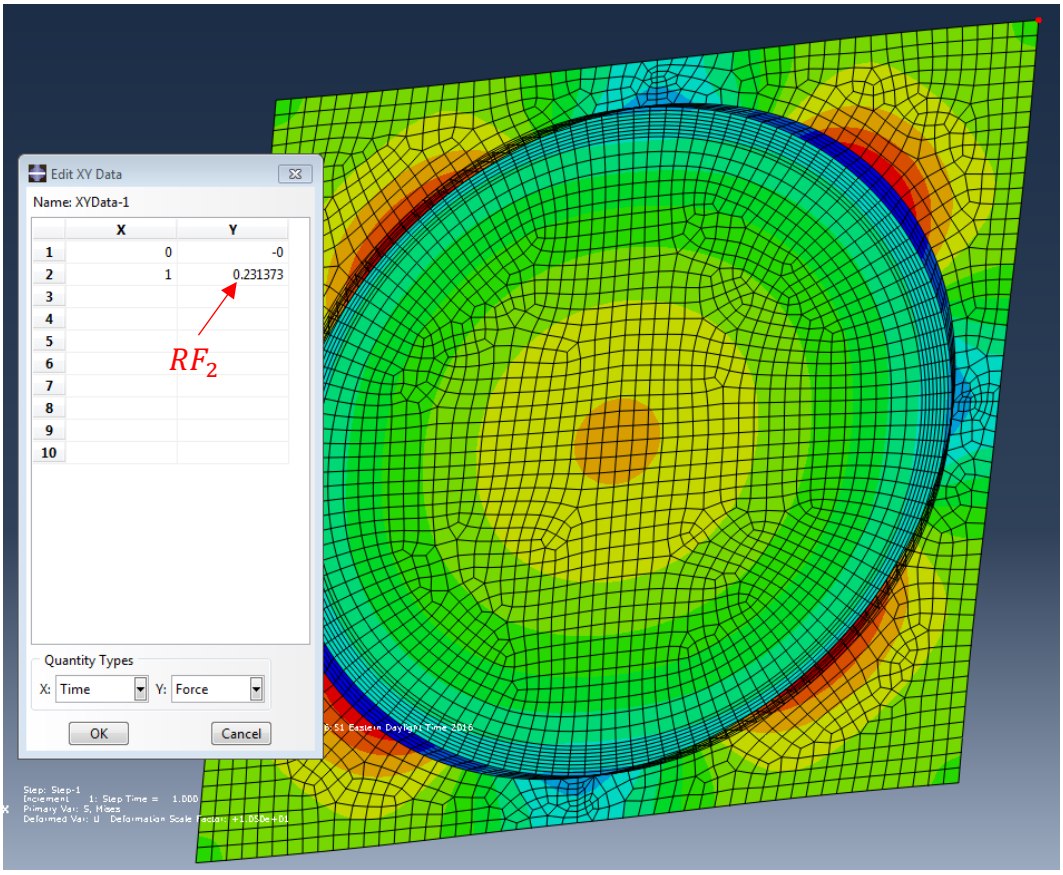

Fig. 6 The second component of the total reaction force (RF_2) acting on the top boundary surface.

2.3.3 Calculation of G_{23}^*

The boundary conditions for the calculation of G_{23}^* are set in such a way that all mechanical strains except $\bar{\varepsilon}_{23}$ are set to zero. The macroscopic transverse shear strain $\bar{\varepsilon}_{23}$=$\bar{\varepsilon}_{32}$ are applied in the following way

$$u_2^{3+} - u_2^{3-} = \bar{\varepsilon}_{23}\Delta x_3 \quad \text{and} \quad u_3^{2+} - u_3^{2-} = \bar{\varepsilon}_{32}\Delta x_2 \tag{12}$$

where the engineering shear strain is applied as $\bar{\gamma}_{23} = 2\bar{\varepsilon}_{23} = 0.02$. The average transverse shear stress $\bar{\sigma}_{23}$ is calculated as

$$\bar{\sigma}_{23} = \frac{RF_2}{A^{3+}} \tag{13}$$

Where A^{3+} is the area of the top boundary surface and equal to 0.1 mm^2; RF_2 is 2 component of total reaction force acting on A^{3+} and equal to 0.231373 N as shown in Fig. 6. Finally, G_{23}^* is equal to $G_{23}^* = {\bar{\sigma}_{23}}/{\bar{\gamma}_{23}}$ =115.6865 GPa.

2.3.3 Calculation of G_{12}^* *and* G_{13}^*

Since the fiber is in square array, the two longitudinal shear moduli are identical, namely, $G_{12}^* = G_{13}^*$. In order to compute G_{12}^* or G_{13}^*, the only non-zero macroscopic longitudinal shear strain $\bar{\gamma}_{12}$ is imposed as

$$u_1^{2+} - u_1^{2-} = \bar{\varepsilon}_{12}\Delta x_2 \quad \text{and} \quad u_2^{1+} - u_2^{1-} = \bar{\varepsilon}_{21}\Delta x_1 \tag{14}$$

where the engineering shear strain is prescribed as $\bar{\gamma}_{12} = 2\bar{\varepsilon}_{12} = 0.02$. The average transverse shear stress $\bar{\sigma}_{12}$ is calculated as

$$\bar{\sigma}_{12} = \frac{RF_1}{A^{2+}} \tag{13}$$

where A^{2+} is the area of the right side boundary surface and equal to 0.1 mm^2; RF_1 is 1 component of total reaction force acting on A^{2+} and equal to 0.235161 N as shown in Fig. 7. Finally, G_{12}^* is equal to $G_{12}^* = {\bar{\sigma}_{12}}/{\bar{\gamma}_{12}}$ =117.5805 GPa.

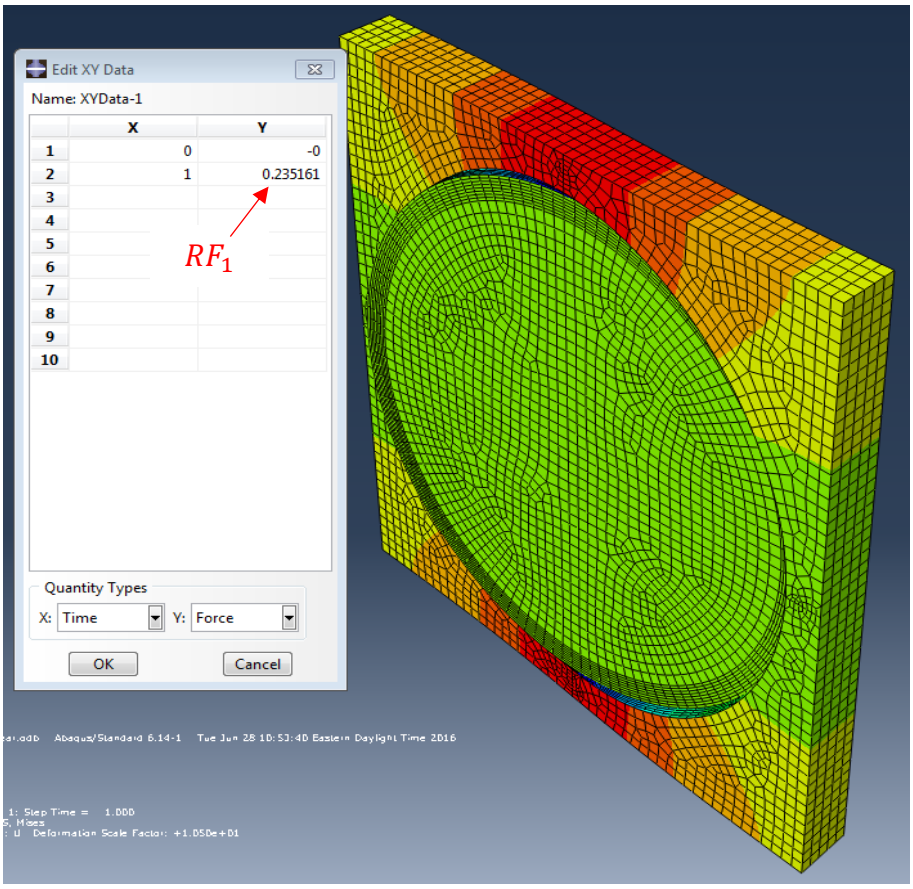

Fig. 7 The first component of the total reaction force (RF_1) acting on the right side boundary surface.

2.3.4 Calculation of thermal expansion coefficients

To evaluate the thermal expansion coefficients, the symmetric boundary conditions are also needed to impose on 1-3, 2-3, and 1-2 planes, respectively, as shown in Fig. 2. All other surfaces are free to move but kept as plane during deformation. The temperature deviation of the unit cell is uniformly increased by $\theta = 1$℃. The effective coefficients of thermal expansion can be obtained by tracking the displacement of corner node as shown in Fig. 8. In this case, the displacement components of the corner node are respectively u_1=2.1616e-6 mm and u_2=u_3=3.20871e-5 mm such that the effective coefficients of thermal expansion are calculated as

$$\alpha_{11}^* = \frac{u_1}{\Delta x_1 \theta} = 21.616\text{e-}6$$

$$\alpha_{22}^* = \alpha_{33}^* = \frac{u_2}{\Delta x_2 \theta} = \frac{u_3}{\Delta x_3 \theta} = 32.0871\text{e-}6$$

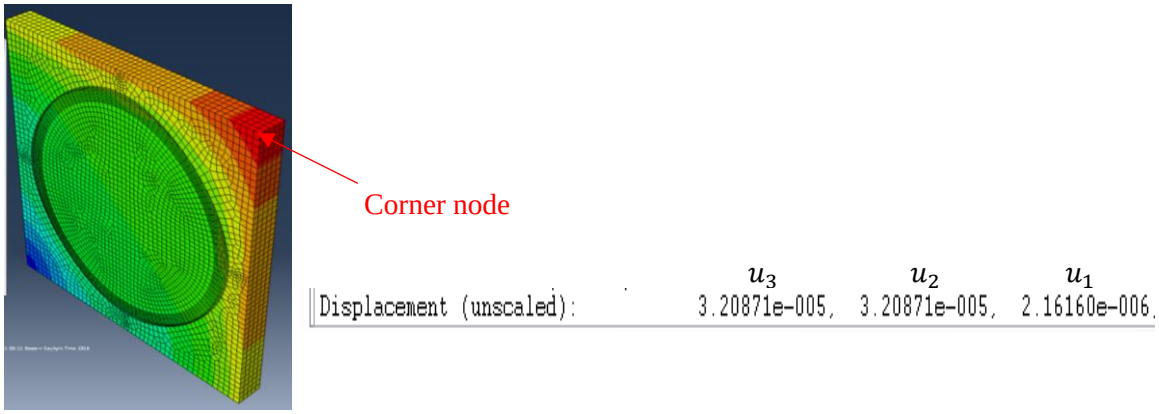

Fig. 8 Contour plot of displacement of unit cell due to thermal expansion and the displacement of the corner node.

Table 2 Effective thermo-mechanical properties predicted by ABAQUS and SwiftComp.

Model	E_{11}^* (GPa)	$E_{22}^* = E_{22}^*$ (GPa)	$G_{12}^* = G_{13}^*$ (GPa)	G_{23}^* (GPa)	$\upsilon_{12}^* = \upsilon_{13}^*$	υ_{23}^*
ABAQUS	406.557	276.84	117.58	115.6865	0.17458	0.203529
SwiftComp	406.557	276.84	117.58	115.6885	0.17458	0.203528
Model	α_{11}^* (μ/℃)	$\alpha_{22}^* = \alpha_{33}^*$ (μ/℃)				
ABAQUS	21.616	32.0871				
SwiftComp	21.616	32.0868				

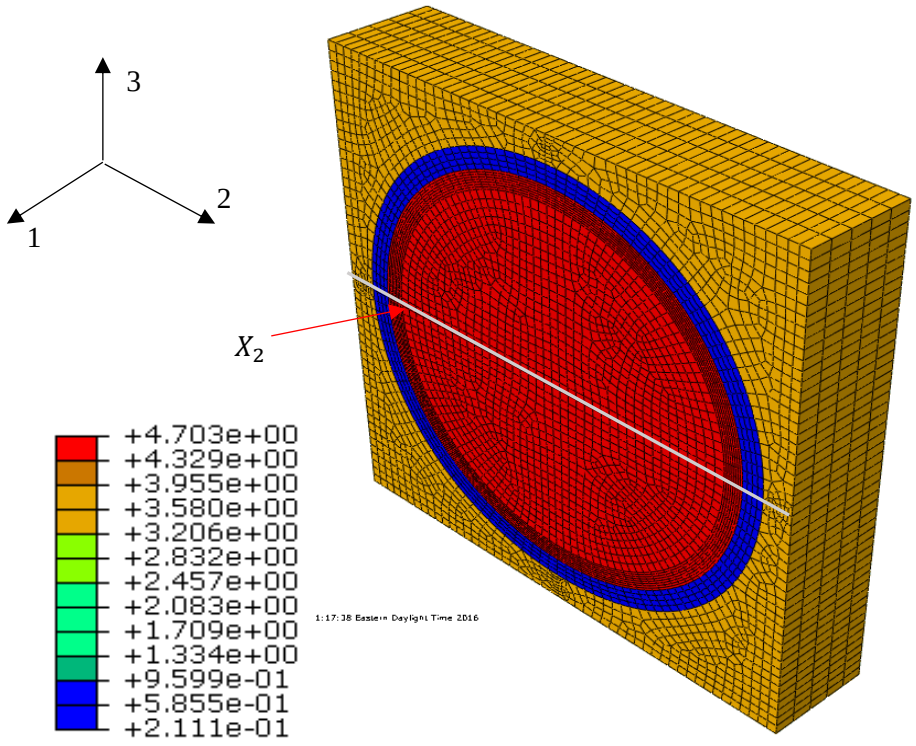

Fig. 9 Contour plot of σ_{11} of the unit cell subjected to $\bar{\varepsilon}_{11} = 0.01$ while all other macroscopic strains are zero.

We also predicted these effective properties using SwiftComp. For comparison the predictions of ABAQUS and SwiftComp are listed in Table 2 together. Obviously, both approaches provide almost identical results.

3. Dehomogenization

Dehomogenization is also called localization which is the method used to recover the distribution of local fields according to different applied macroscopic loadings. Finite element unit cell model need to recalculate the local fields based on the prescribed macroscopic loading. Fig. 9 shows the contour plot of stress σ_{11} of the unit cell

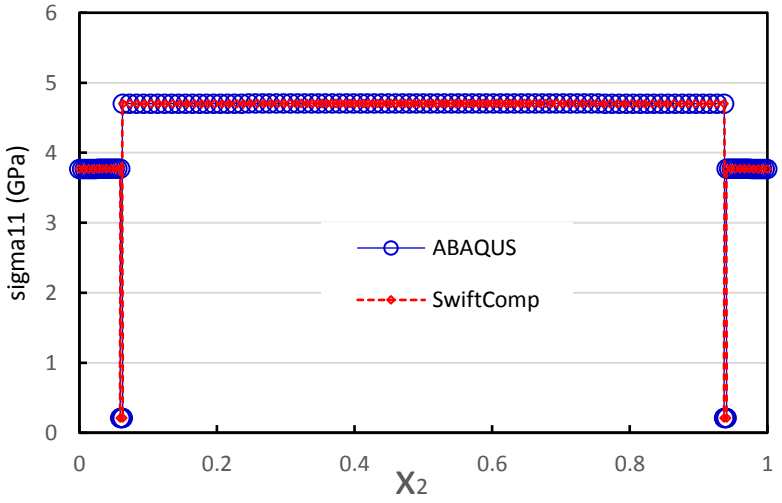

Fig. 10 The distribution of stress component σ_{11} along the center line X_2 predicted by ABAQUS and SwiftComp when the only non-zero macroscopic strain is $\bar{\varepsilon}_{11} = 0.01$.

subjected to $\bar{\varepsilon}_{11} = 0.01$ while all other macroscopic strains are zero. The detailed stress distributions of σ_{11} along the center line X_2 as shown in Fig. 9 calculated by ABAQUS and SwiftComp are plotted in Fig. 10 together. Furthermore, the distributions of stress components σ_{22} and σ_{33} are plotted in Fig. 11 (a-b) when the unit cell is subjected to macroscopic strain $\bar{\varepsilon}_{22} = 0.01$ which is the only non-zero strain. Fig. 12 presents the distribution of stress components σ_{33} which the unit cell is subjected to $\bar{\varepsilon}_{11} = \bar{\varepsilon}_{13} = 0.01$. One can observe from Fig. 10-12 that the predictions provided by both approaches have excellent agreement.

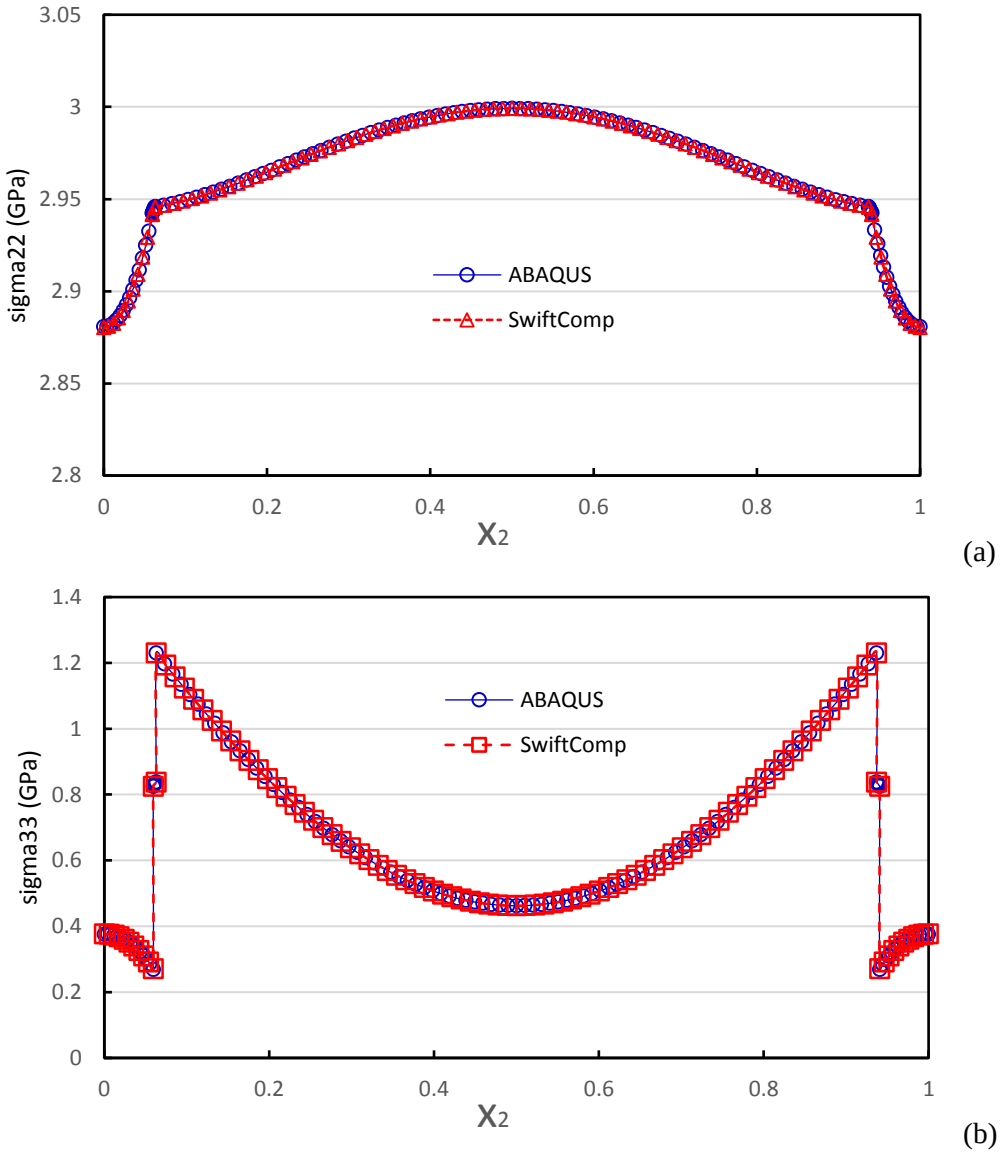

Fig. 11 The distribution of stress component (a) σ_{22}, and (b) σ_{33} along the center line X_2 calculated by ABAQUS and SwiftComp when the unite cell is subjected to macroscopic strain is $\bar{\varepsilon}_{22} = 0.01$ while other mechanical strains are zero.

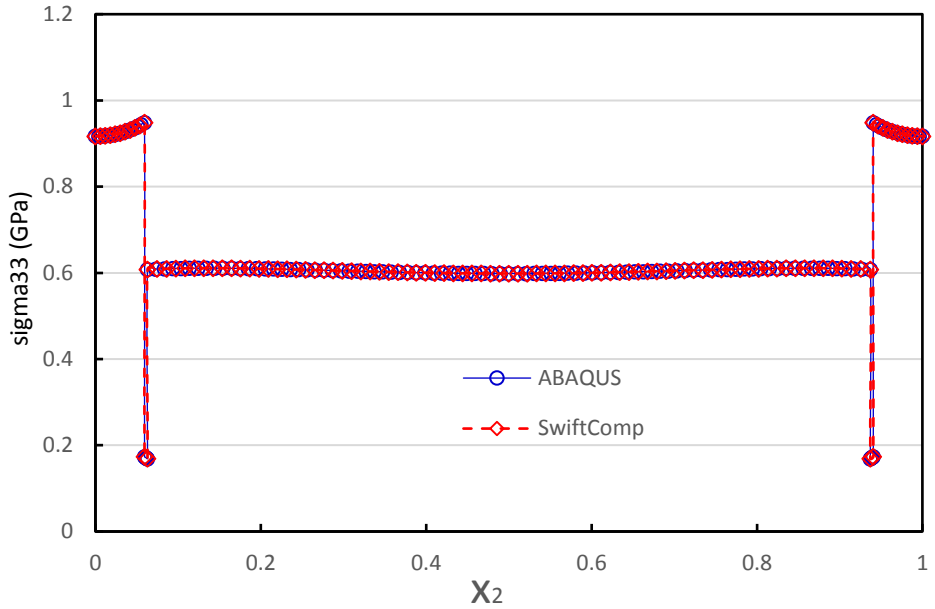

Fig. 12 The distribution of stress component σ_{33} along the center line X_2 predicted by ABAQUS and SwiftComp when the unit cell was simultaneously applied by the macroscopic strains $\bar{\varepsilon}_{11} = \bar{\varepsilon}_{13} = 0.01$.